

More is not always better: modeling the effects of elastic exoskeleton compliance on underlying ankle muscle–tendon dynamics

This content has been downloaded from IOPscience. Please scroll down to see the full text.

2014 Bioinspir. Biomim. 9 046018

(<http://iopscience.iop.org/1748-3190/9/4/046018>)

View [the table of contents for this issue](#), or go to the [journal homepage](#) for more

Download details:

IP Address: 152.14.127.138

This content was downloaded on 24/11/2014 at 15:50

Please note that [terms and conditions apply](#).

# More is not always better: modeling the effects of elastic exoskeleton compliance on underlying ankle muscle–tendon dynamics

Benjamin D Robertson<sup>1</sup>, Dominic J Farris<sup>1,2</sup> and Gregory S Sawicki<sup>1</sup>

<sup>1</sup> Joint Department of Biomedical Engineering, University of North Carolina-Chapel Hill and North Carolina State University, EB3-Room 4130, 911 Oval Drive, Campus Box 7115, Raleigh, NC 27695, USA

<sup>2</sup> School of Human Movement Studies, Level 5, Human Movement Studies Building (26B), Blair Drive, The University of Queensland, St Lucia QLD 4072, Australia

E-mail: [bdrober3@ncsu.edu](mailto:bdrober3@ncsu.edu)


Received 10 April 2014, revised 19 June 2014

Accepted for publication 25 July 2014

Published 24 November 2014

## Abstract

Development of robotic exoskeletons to assist/enhance human locomotor performance involves lengthy prototyping, testing, and analysis. This process is further convoluted by variability in limb/body morphology and preferred gait patterns between individuals. In an attempt to expedite this process, and establish a physiological basis for actuator prescription, we developed a simple, predictive model of human neuromechanical adaptation to a passive elastic exoskeleton applied at the ankle joint during a functional task. We modeled the human triceps surae–Achilles tendon muscle tendon unit (MTU) as a single Hill-type muscle, or contractile element (CE), and series tendon, or series elastic element (SEE). This modeled system was placed under gravitational load and underwent cyclic stimulation at a regular frequency (i.e. hopping) with and without exoskeleton (Exo) assistance. We explored the effect that both Exo stiffness ( $k_{\text{Exo}}$ ) and muscle activation ( $A_{\text{stim}}$ ) had on combined MTU and Exo (MTU + Exo), MTU, and CE/SEE mechanics and energetics. Model accuracy was verified via qualitative and quantitative comparisons between modeled and prior experimental outcomes. We demonstrated that reduced  $A_{\text{stim}}$  can be traded for increased  $k_{\text{Exo}}$  to maintain consistent MTU + Exo mechanics (i.e. average positive power ( $\bar{P}_{\text{mech}}^+$ ) output) from an unassisted condition (i.e.  $k_{\text{Exo}} = 0 \text{ kN} \cdot \text{m}^{-1}$ ). For these regions of parameter space, our model predicted a reduction in MTU force, SEE energy cycling, and metabolic rate ( $\bar{P}_{\text{met}}$ ), as well as constant CE  $\bar{P}_{\text{mech}}^+$  output compared to unassisted conditions. This agreed with previous experimental observations, demonstrating our model's predictive ability. Model predictions also provided insight into mechanisms of metabolic cost minimization, and/or enhanced mechanical performance, and we concluded that both of these outcomes cannot be achieved simultaneously, and that one must come at the detriment of the other in a spring-assisted compliant MTU.

 Online supplementary data available from [stacks.iop.org/BB/9/046018/mmedia](http://stacks.iop.org/BB/9/046018/mmedia)

Keywords: elastic ankle exoskeleton, muscle–tendon interaction, mechanics, energetics, hopping, ultrasound

(Some figures may appear in colour only in the online journal)

## Introduction

In the last two decades, significant progress has been made towards developing functional wearable robotic devices to assist/enhance human locomotion [1]. The majority of these devices rely on powered actuation to effectively assist the wearer through a conventional rigid [2–7] or (more recently) soft/elastic [8] robotic interface. Unfortunately, powered devices are either restricted to a laboratory setting [4, 6, 7], or carry a significant added mass penalty [2, 3, 5, 8], which offsets most, if not all, of the mechanical/energetic benefit the device may provide. Recently, however, there has been a shift towards development of unpowered passive (i.e. spring driven) exoskeletons, as these devices can provide increased limb/joint stiffness/torque with minimal added mass penalty [9–11].

The rationale underlying application of springy actuators for locomotion assistance is not limited to decreasing device weight and power consumption, it also makes sense from a mechanical perspective. Humans employ ‘bouncing’ gait patterns during walking, running, and hopping; and it has been demonstrated that the center of mass mechanics in each of these modes of gait can be predicted by treating the leg as a simple spring-loaded inverted pendulum [12–15]. Elastic mechanics are not exclusive to the whole limb behavior, and there are multiple reports of muscle level mechanics that facilitate energy storage and return in series compliant tissues (e.g. tendon and aponeurosis) spanning the ankle joint during walking [16–20], running [16–19], hopping [21, 22], and bouncing [23, 24]. Given the spring-like behavior at the whole limb and joint level, passive exoskeleton actuation is uniquely well-suited to integration with existing limb mechanics.

There have been several studies that illustrate the effectiveness of springy actuators for assisting functional movement [21, 22, 25–27]. Grabowski and Herr [26] demonstrated that a spring-actuated exoskeleton spanning all three joints of the lower limb could reduce the metabolic demands of hopping in place. Their study participants achieved this by reducing biological contributions to limb stiffness and utilizing the parallel springs for energy storage and return; all while keeping center of mass and whole-limb plus exoskeleton mechanics consistent with limb mechanics observed during unassisted hopping [26].

Similar studies conducted with springy exoskeletons spanning only the ankle demonstrated that this effect scales, and that humans modulate muscle activation and biological stiffness to maintain joint-level and whole limb stiffness [27]. Plantar-flexor muscle groups generally decreased activation levels when assistance was provided by a wearable device, thereby reducing force production [21, 22, 25, 27]. This ultimately affects the function of series compliant tissues (e.g. tendon, aponeurosis) known to cycle large amounts of energy during bouncing gait [12, 16–20, 23, 28, 29].

A recent muscle-level ultrasound study demonstrated that a spring assisted exoskeleton facilitated decreased soleus muscle force production in conjunction with increases in soleus fascicle excursion [22]. This had a net effect of

maintaining a constant level of muscle average positive mechanical power ( $\bar{P}_{\text{mech}}^+$ ) output. The Achilles tendon, however, experienced a large decrease in energy cycling which ultimately resulted in reduced MTU  $\bar{P}_{\text{mech}}^+$  [22]. Despite this, it has been demonstrated that these ‘detuned’ mechanics can result in reduced metabolic rates [21, 22]. These reductions only hold to a point, though. As Grabowski *et al* demonstrated, more exoskeleton stiffness can decrease (or even eliminate) the metabolic benefits of a spring-actuated exoskeleton [26].

While it is clear that some exoskeleton assistance can be beneficial [21, 22, 26], and too much can be counter-productive or even detrimental [26], very little has been done to examine how muscle architecture and system mechanics can be *optimally* assisted by a springy actuator. For this to be possible, a broader understanding of how exoskeleton stiffness ( $k_{\text{Exo}}$ ) impacts neuromechanical and energetic function at the muscle level is required. With this in mind we present a simplified model of the triceps surae–Achilles tendon complex with parallel spring-actuated assistance during simulated human hopping. Based on previous findings from human studies, we predicted our model would (1) be able to trade reduced muscle activation for increased  $k_{\text{Exo}}$  to maintain system (i.e. MTU + Exo) level stiffness and  $\bar{P}_{\text{mech}}^+$  production [27]. Given constant MTU + Exo  $\bar{P}_{\text{mech}}^+$  output but increasing spring stiffness, we predicted (2) increased  $\bar{P}_{\text{mech}}^+$  output from the Exo component, as well as decreased output from the MTU and SEE components of the biological system would occur with increasing  $k_{\text{Exo}}$  [21, 22, 25, 26]. Despite reductions in loading of biological components with increasing  $k_{\text{Exo}}$ , we hypothesized that (3) the contractile element (CE) would maintain constant  $\bar{P}_{\text{mech}}^+$  output by increasing its excursion in conjunction with reduced force [22]. Finally, we predicted that (4) these changes in system and component level mechanics would ultimately result in a reduced metabolic expenditure when springy assistance is provided [21, 22, 26].

## Methods

### *Hopping as a model of functional ankle mechanics*

We chose to model hopping in this study because it is a primarily ankle driven mode of bouncing gait that is simple both mechanically, and from a neural control perspective [21, 30]. Despite its inherent simplicity, however, hopping captures one of the critical features of all bouncing gait: the ability to store and return energy in series tendon at distal joints [22, 23]. Using hopping as a model of functional ankle joint mechanics allowed us to ask fundamental questions concerning the impact of passive exoskeleton assistance on the mechanics and energetics of biological muscle–tendon unit in a simple, straightforward way. Finally, hopping comes with a wealth of experimental whole limb [26, 27], joint-level [21, 25–27], muscle level [22], electromyographic [21, 22, 25], and metabolic [21, 22, 26] data to compare model predictions against.

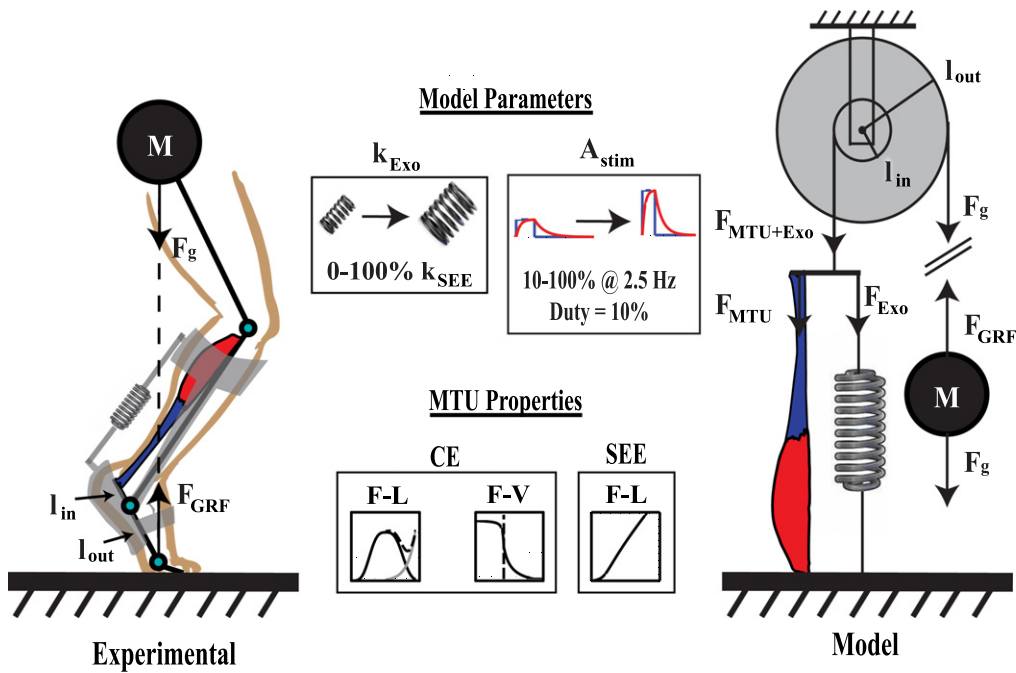


**Figure 1** Experimental (left) and modeled (right) exoskeleton assisted human hopping. Range of stimulation and exoskeleton parameters explored here (top), as well as CE/SEE actuation properties (bottom) are indicated in boxes. The  $A_{stim}$  parameter acts on biological muscle, and  $k_{Exo}$  is the stiffness of the modeled parallel passive exoskeleton.

*Biological muscle tendon unit model*

Our modeled muscle–tendon unit (MTU) consisted of a single Hill-type CE subject to nonlinear force–length ( $F-L$ ) and –velocity ( $F-V$ ) actuation dynamics (figure 1); as well as first order activation dynamics. It also had a parallel elastic element capable of generating passive force at lengths greater than  $l_0$ , the length at which active muscle produces its peak isometric force [31] (figure 1). Parameterization of normalized  $F-L$  characteristics was based on experimental observation in Rubenson *et al* [32]. Normalized  $F-V$  and first order activation dynamics were based on parameterized equations from Haeufle *et al* [33]. Tendon/series elastic element (SEE) dynamics were modeled based on observations from Lichtwark *et al* [18], and exhibited a nonlinear ‘toe’ region, after which dynamics can be approximated as linear. All model equations and parameter values used here are detailed in supplementary text.

*Inertial environment*

System inertial mechanics were modeled by assuming a single rigid attachment point of the biological MTU and exoskeleton (Exo) system to lever arm acting with a fixed mechanical advantage (i.e. pulley) on a point mass under constant gravitational load. This was meant to reflect loading experienced by the triceps surae–Achilles tendon complex at the ankle joint during human hopping (figure 1). Rationale and justification for using this simplified inertial environment are discussed further in Robertson *et al* [34].

*Model simplifications*

Several key simplifications were made to facilitate implementation of this modeling framework. First, the gastrocnemii and soleus muscle of the triceps surae–Achilles tendon complex were lumped into a single, mono-articular, fusiform muscle. This facilitated use of a simplified limb geometry, and disregards complications that arise from having biarticular and bipennate (i.e. non-fusiform) gastrocnemii muscles (figure 1). While, based on physiological cross-sectional area (PCSA), soleus is the primary force producer within the triceps surae muscle group, these simplifications likely diminished the potential impact that gastrocnemii operating point and architecture played in governing adaptation at the ankle and knee in humans during spring assisted hopping [21, 22]. Secondly, our system operates with a fixed mechanical advantage, disregarding shifts in biological moment arm length that can occur *in vivo* [35, 36]. Finally, all muscle fibers were assumed to have identical activation/deactivation time constants ( $\tau_{act}$  and  $\tau_{deact}$  respectively), and values used in first order activation dynamics are a weighted average of observed values based on muscle PCSA in cadavers [37–39]. Further justification of model simplifications can be found in Robertson *et al* [34].

*Modeled exoskeleton*

Our model of human hopping with exoskeleton assistance had a linear tension spring in parallel with the biological MTU (figure 1). The slack length of our modeled exoskeleton was the combined length at which the inactive CE developed passive force ( $l_0$ ), and slack length of SEE complex ( $l_{slack}$ ). The exoskeleton moment arm length is the same as that of the

biological MTU ( $l_{in} = 0.04$  m) [37]. This was done to simplify scaling of relative Exo/MTU stiffness relationships explored in this study. We note that stiffness comparisons can be extended to systems where exoskeleton and biological moment arms are not equal by converting linear stiffness ( $\text{N m}^{-1}$ ) to rotational stiffness ( $\text{N m rad}^{-1}$ ) using the following relationship

$$k_{\theta} = k_x \cdot (l_{in})^2,$$

where  $k_{\theta}$  is rotational stiffness,  $k_x$  is linear stiffness, and  $l_{in}$  is the distance from the point where force is applied to the center of joint rotation (i.e. moment arm) (figure 1). Finally, transmission of assistive forces was presumed to be ideal, and no attempt was made to model interaction of rigid exoskeleton with soft tissue.

### Experimental protocol

The model stimulation frequency ( $\omega_{stim}$ ) was 2.5 Hz, a frequency at which metabolic cost was consistently reduced in human experiments examining exoskeleton assisted hopping [21, 22, 26].  $k_{Exo}$  was varied in  $4.5 \text{ kN m}^{-1}$  (2.5%  $k_{SEE}$ ) increments from unassisted ( $k_{Exo} = 0 \text{ N m}^{-1}$ ) to that of biological tendon ( $k_{SEE} = 180 \text{ kN m}^{-1}$ ), corresponding to joint level stiffness during perfectly isometric unassisted hopping (i.e.  $k_{MTU} = k_{SEE}$ ). Stimulation was provided as a square wave pulse with 10% duty relative to  $\omega_{stim}$  (i.e.  $T_{pulse} = 0.1 \times \omega_{stim}^{-1}$ ). This pulse was subject to first order activation dynamics exhibited by biological muscle [31]. Stimulation amplitude ( $A_{stim}$ ) ranged from 10% to 100% of maximum possible. All modeled conditions were run for 15 s (~37 hops) to allow time for the system to become stable and cyclic. For each  $A_{stim}/k_{Exo}$  combination, the final 4 complete hopping cycles were used in all subsequent analysis. Parameter values and equations used in model implementation are detailed in supplementary material.

### Experimental metrics

The major criterion for a simulation to successfully ‘hop’ included having a flight phase where the MTU + Exo system went slack, and the only force applied to our virtual mass was gravity (i.e.  $F_{net} = F_g$ ). Potential risk of injury was also taken into account as part of determining a successful hop, and normalized peak CE strains ( $\epsilon_{peak}$ ) > 0.3 were assumed to pose significant risk of injury based on reports from literature [40–42].  $\epsilon_{peak}$  was computed as follows

$$\epsilon_{peak} = \frac{\left( \max_{t=0 \rightarrow T_{stim}} (l_{CE}(t)) - l_0 \right)}{l_0},$$

where the cycle period  $T_{stim} = \omega_{stim}^{-1}$  and  $l_{CE}(t)$  was CE length as a function of time. Finally, successful hopping was required to be cyclic with stimulation, and show no variance when subjected to the integrated return map method detailed in [34].

Once it had been determined that a given condition meets the criterion for hopping in a safe and effective manner, system and component level analysis of mechanics and energetics was performed. First, we determined average positive power over a cycle of hopping for the system (i.e. MTU + Exo) and its respective mechanical components (i.e. MTU, active/passive CE, SEE, Exo) as follows

$$\bar{P}_{mech}^+ = \frac{1}{T_{stim}} \times \int_{t=0}^{T_{stim}} P_{mech}^+(t) dt,$$

where

$$P_{mech}^+(t) = \begin{cases} 0 & \text{when } v(t) > 0, \\ P_{mech}(t) & \text{when } v(t) < 0. \end{cases}$$

In other words, power output was positive for shortening (i.e. work done against gravity).

Next, we explored system peak force ( $F_{peak}$ ) over a cycle of hopping

$$F_{peak} = \max_{t=0 \rightarrow T_{stim}} (F_{MTU+Exo}(t)) = F_{MTU+Exo}(t_{peak}),$$

where  $F_{MTU+Exo}(t)$  is MTU + Exo force as a function of time, and  $t_{peak}$  is the time point within a cycle where peak system (MTU + Exo) force occurs. We were also interested in how the MTU, Exo, and active/passive CE components shared loads at  $t_{peak}$  and computed their respective forces as well.

We were also concerned with how CE  $F$ - $L$  and  $F$ - $V$  dynamics influenced system mechanics, so we computed the range and average operating strains/velocities from stimulation onset (muscle activation,  $\alpha(t) > 0$ ) to the initiation of flight ( $F_{MTU+Exo}(t) = F_g$ ). Note that this does not include any passive stretch prior to stimulation onset, and only encompassed portions of ground contact where *active* muscle was likely to make significant contributions.

We were also interested in system energetics, and calculated average metabolic rate ( $\bar{P}_{met}$ ) using a dimensionless model of metabolic cost [43, 44] as a function of muscle velocity scaled by physiological constants  $F_{max}$  (the maximum active isometric CE force),  $v_{max}$  (maximum CE shortening velocity), (supplemental text table 1), and normalized muscle active state  $\alpha(t)$  [45].  $\bar{P}_{met}$  was computed as follows

$$\bar{P}_{met} = \frac{1}{T_{stim}} \times F_{max} \times v_{max} \times \int_{t=0}^{T_{stim}} [\alpha(t) \times p_{met}(v_{CE}(t)/v_{max})] dt,$$

where  $p_{met}(v_{CE}(t)/v_{max})$  is dimensionless metabolic cost at time  $t$  from [1] (supplemental text table 2). MTU + Exo, MTU, and CE apparent efficiency ( $e_{app}$ ) were also a focus of this study, and were computed as follows based on their respective  $\bar{P}_{mech}^+$  output

$$e_{app} = \bar{P}_{mech}^+ / \bar{P}_{met}.$$

Further details on equations, metrics, and constants used as part of model implementation and subsequent analysis can be found in supplementary text.

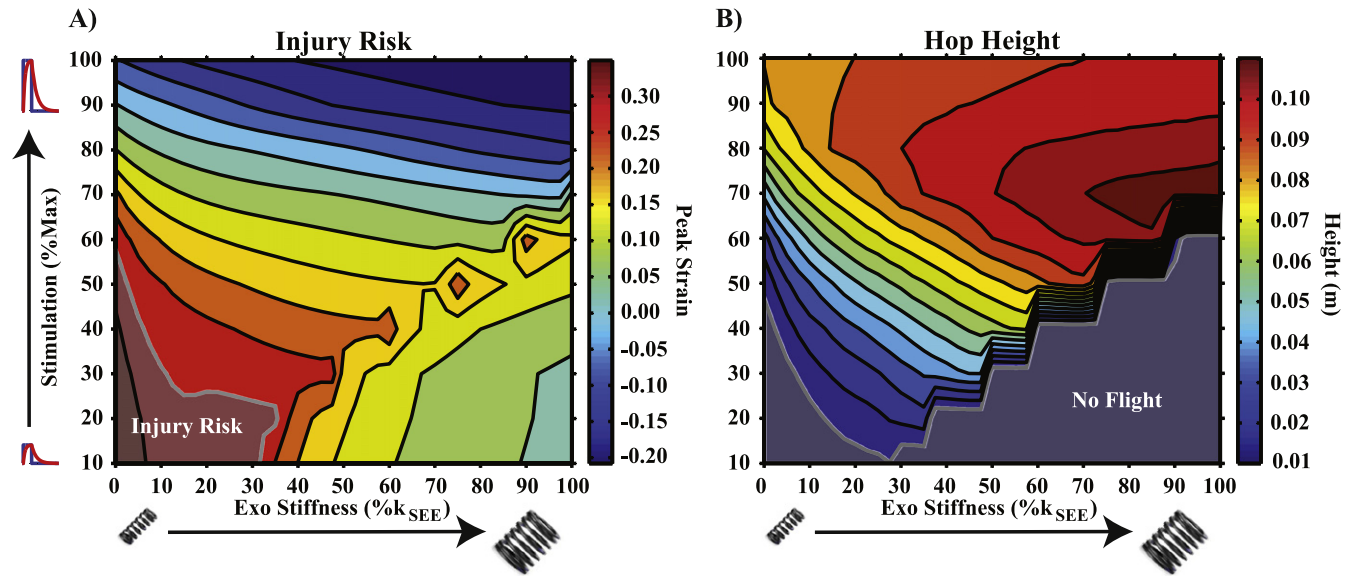


**Figure 2** (A) Contour of peak eccentric strain over a cycle of hopping. Regions exceeding a value of 0.3 or greater were indicated by opaque region labeled ‘injury risk.’ (B) Contour of peak height achieved over a cycle of hopping. Regions where flight height  $\approx 0$  were indicated by the opaque region labeled ‘no flight.’

### Comparison to experimental data

Experimental data used in all quantitative comparisons made here were taken from Farris *et al* [21]. Exoskeleton rotational stiffness used in experimental conditions was  $91 \text{ N m rad}^{-1}$  which, when scaled by our modeled biological ‘in’ moment arm (0.04 m) [37] and converted to  $\text{kN m}^{-1}$  yields  $\sim 56 \text{ kN m}^{-1}$ . We constrained our selection of points based on experimental conditions (i.e. unassisted/ $k_{\text{Exo}} = 0 \text{ kN m}^{-1}$  and assisted/ $k_{\text{Exo}} \approx 54\,000 \text{ kN m}^{-1}$ ), and matched MTU + Exo and MTU average positive power to experimental data for the whole ankle joint with and without an exoskeleton [21]. We selected these two metrics as a basis for comparison because our simplified model does not have the necessary geometric/physiological complexity for quantitative comparisons to muscle level data observed in [22].

## Results

### Stability, injury risk, and flight phase

For all modeled conditions, stable and cyclic mechanics were easily achieved within the time allotted, and the final 4 cycles used in analysis are all representative of steady-state behavior. Significant risk of injury was observed for low  $A_{\text{stim}}$ , low  $k_{\text{Exo}}$  combinations. These regions exhibited CE peak eccentric strains  $> 0.3$  at some point in their hopping cycle (figure 2(A)) [40–42].

A flight phase was achieved for the majority of the parameter space, with notable exceptions for low  $A_{\text{stim}}$  ( $< 20\%$  of max) low  $k_{\text{Exo}}$  ( $< 20\%k_{\text{SEE}}$ ) combinations, as well as low-to-medium  $A_{\text{stim}}$  ( $< \sim 50\%$  of max) and high  $k_{\text{Exo}}$  ( $> \sim 50\%k_{\text{SEE}}$ ) conditions. The greatest flight amplitude

was observed at  $70\% A_{\text{stim}}$  and high  $k_{\text{Exo}}$  ( $> 70\%k_{\text{SEE}}$ ) conditions (figure 2(B)).

Regions where elevated injury risk or no flight phase were observed are indicated by opaque regions labeled ‘Injury Risk’ and ‘No Flight’ in figures 2(A) and (B) respectively and all subsequent contour plots (figures 3(A), (C) and 6(A)–(C)).

### Average positive power

Maximal MTU + Exo  $\bar{P}_{\text{mech}}^+$  was generated for high  $A_{\text{stim}}$ , high  $k_{\text{Exo}}$  conditions (figure 3(A)). Minimums in MTU + Exo  $\bar{P}_{\text{mech}}^+$  were generally observed for low stimulation amplitudes regardless of  $k_{\text{Exo}}$  (figure 3(A)). Data points from a contour of constant Exo + MTU  $\bar{P}_{\text{mech}}^+$  spanning  $100\% A_{\text{stim}}$  with no exoskeleton (i.e.  $k_{\text{Exo}} = 0 \text{ kN m}^{-1}$ ) through  $50\% A_{\text{stim}}$  and an  $k_{\text{Exo}} = 90 \text{ kN m}^{-1}$  (i.e.  $k_{\text{Exo}} = 50\%k_{\text{SEE}}$ ) were selected for further analysis, and are indicated by white dots in all subsequent contours (figure 3(A)). MTU + Exo workloops from data during ground contact were generated for these selected points and are visualized in figure 3(B).

In general, CE  $\bar{P}_{\text{mech}}^+$  was highest for low  $A_{\text{stim}}$ /high  $k_{\text{Exo}}$  combinations along the border of the ‘no flight’ region (figure 3(C)), and lowest for high  $A_{\text{stim}}$ / $k_{\text{Exo}}$  conditions where a flight phase was safely achieved (figure 3(C)). Ground contact CE workloops for selected points from figure 3(A) are visualized in figure 3(D).

### Force and power sharing

Selected points of constant MTU + Exo  $\bar{P}_{\text{mech}}^+$  (figure 3(A)) traded energy cycled in biological tendon for energy cycled in the modeled exoskeleton, dramatically reducing  $F_{\text{MTU}}(t_{\text{peak}})$  and  $\bar{P}_{\text{mech}}^+$  from the biological MTU (figure 4). Maintaining constant MTU + Exo  $\bar{P}_{\text{mech}}^+$  as in figure 3(A) required a slight increase in MTU + Exo  $F_{\text{peak}}$  while simultaneously decreasing

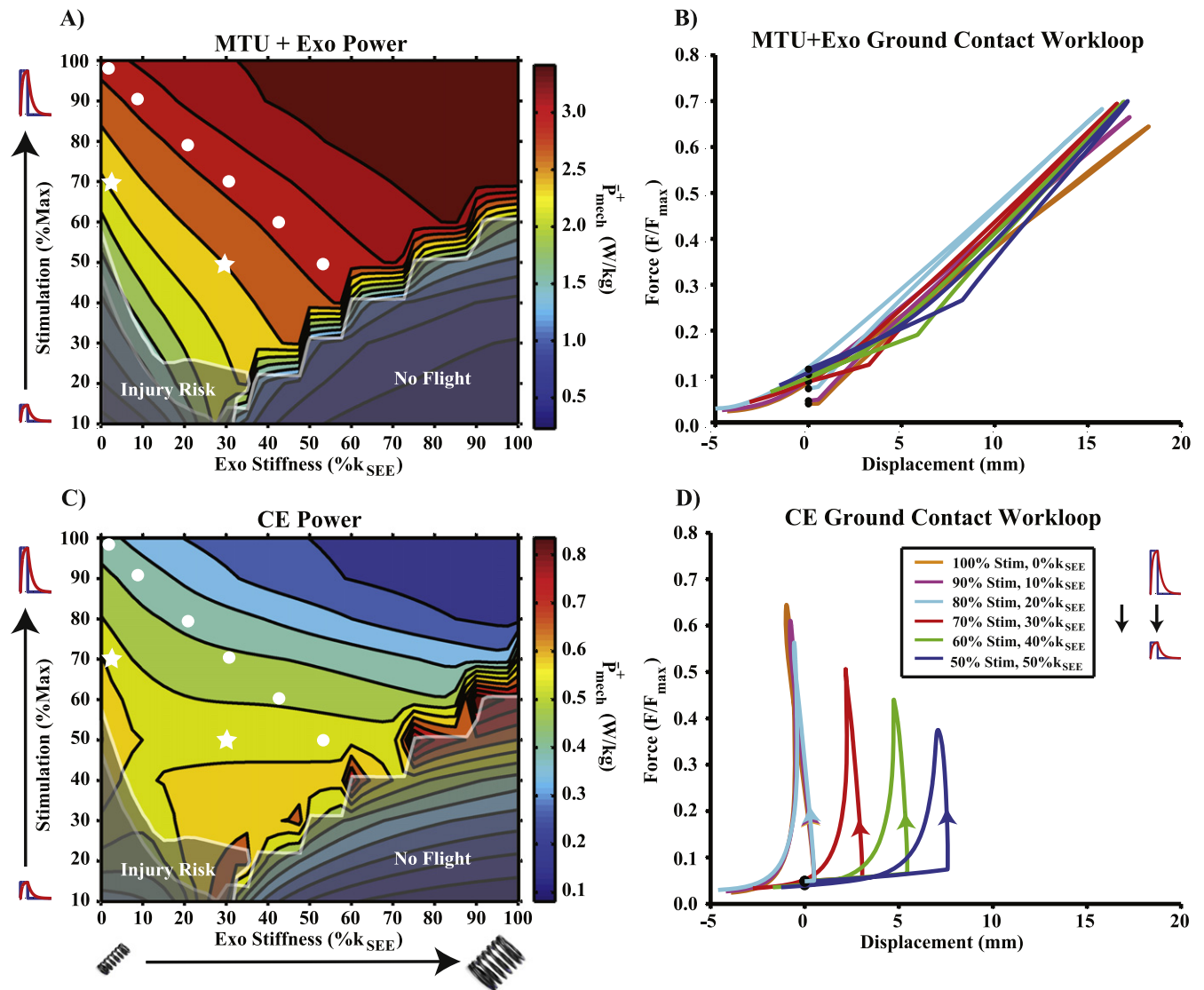


**Figure 3** (A) Average positive power output for the combined MTU + Exo system. White dots in this and all subsequent contour plots indicate points in parameter space of equivalent MTU + Exo positive power. Stars represent points that correspond to joint level mechanics observed in [22]. Note that there were several contours which trade stimulation amplitude for Exo stiffness to achieve constant MTU + Exo positive power output. (B) Workloops during ground contact (i.e.  $F_{MTU+Exo} > 0$ ) for points in parameter space indicated by white dots in (A). The force–displacement profile (i.e. ‘stiffness’) in each case was nearly identical. (C) Contour plot of average positive power produced by the CE (active + passive). (D) CE workloops during ground contact for points in parameter space indicated by white dots. Positive power remained nearly constant by trading decreased force output for increased excursion.

the force burden on the biological MTU (figure 4(A)). Despite reduced  $F_{MTU}(t_{peak})$  with increased  $k_{Exo}$  for selected data points, there was a small increase in contributions to  $F_{peak}$  from passive CE components (figure 4(A)). This had little effect on CE  $\bar{P}_{mech}^+$ , which remained nearly constant for these same points in parameter space. CE power actually *increased* slightly from baseline (unassisted,  $k_{Exo} = 0 \text{ kN m}^{-1}$ ) to high  $k_{Exo}$ , low  $A_{stim}$  conditions for selected points of constant MTU + Exo  $\bar{P}_{mech}^+$  (figure 4(B)).

*Force–length and force–velocity dynamics*

Force–length ( $F$ – $L$ ) and –velocity ( $F$ – $V$ ) operating points during active force production for data points selected in

figure 3(A) can be seen in figure 5. As  $A_{stim}$  decreased and  $k_{Exo}$  increased, the modeled CE increased its range of operating lengths as well as average values of both operating length and velocity (bars, figure 5). Average operating strain increased from approximately  $0.9$ – $1.15l_0$  ( $\sim 4.9$ – $6.3 \text{ cm}$ ) (markers, figure 5(A)), while average operating velocity more than doubled from  $\sim 0.07$  to  $0.16 v_{max}$  ( $\sim 3$ – $7 \text{ cm s}^{-1}$ ) (markers, figure 5(B)).

*Metabolic rate and efficiency*

Average metabolic rate scaled almost directly with  $A_{stim}$  /integrated muscle activation (figure 6(A)), but there was a slight increase in  $\bar{P}_{met}$  when  $A_{stim}$  was held constant and  $k_{Exo}$  was increased (figure 6(A)). For the data points of

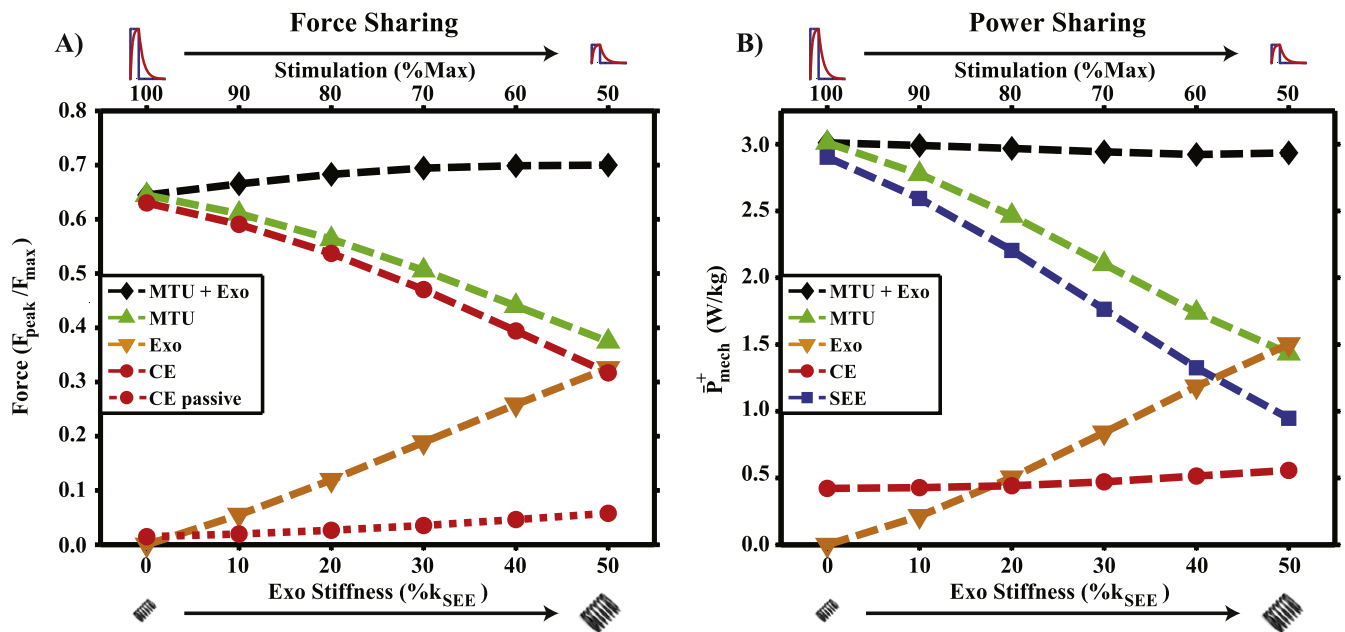


**Figure 4** (A) MTU + Exo peak force and system component contributions for points indicated by white dots in figure 3(A). Biological components are unloaded as Exo contributions rise in conjunction with increased passive contributions from CE. (B) Average positive power output from MTU + Exo and its components for the same points as in (A). System level power remains constant by trading MTU/SEE power output for energy cycled in Exo, while CE positive power remains nearly constant.

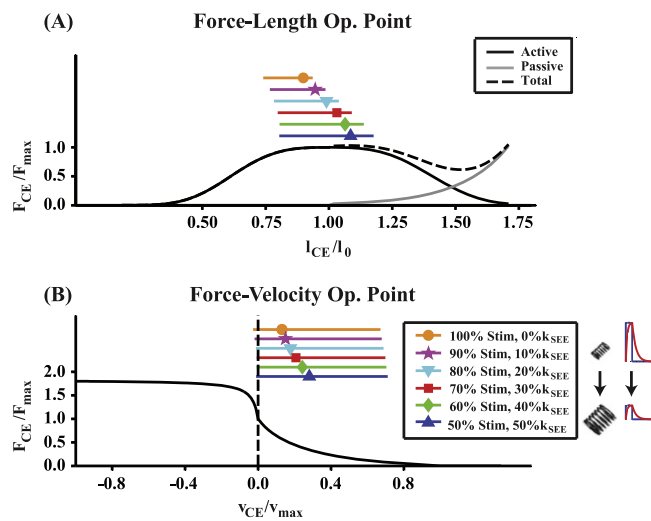


**Figure 5** (A) CE force-length operating point for points in parameter space indicated by white dots in figure 3(A). (B) CE force-velocity operating point for white dot points in figure 3(A). In both figures, markers indicate average operating point, and bar indicates range of operating points. Both average and range of force-length and -velocity operating points increases as stimulation amplitude was decreased and Exo stiffness was increased to maintain constant MTU + Exo average positive power output.

constant MTU + Exo  $\bar{P}_{mech}^+$  selected in figure 3(A),  $\bar{P}_{met}$  decreased with decreasing  $A_{stim}$  and increasing  $k_{Exo}$  (figure 6(A)).

MTU  $e_{app}$  decreased with decreasing  $A_{stim}$  except in low-to-no  $k_{Exo}$  conditions (figure 6(B)). MTU  $e_{app}$  also decreased as  $k_{Exo}$  increased unless  $A_{stim}$  was  $\geq 90\%$  of maximum, at

which point it increased slightly from unassisted (figure 6(B)). For the data points selected in figure 3(A), MTU  $e_{app}$  declined rapidly with decreasing  $A_{stim}$  and increasing  $k_{Exo}$  (figure 6(B)).

CE  $e_{app}$  (active + passive components) generally decreased with increasing  $k_{Exo}$ , and increased with decreasing  $A_{stim}$  (figure 6(C)). For the data points selected in figure 3(A), CE  $e_{app}$  increased with decreased  $A_{stim}$  and increased  $k_{Exo}$  (figure 6(C)).

### Experimental comparison

An MTU  $\bar{P}_{mech}^+$  of  $\sim 2.4 \text{ W kg}^{-1}$  was observed for the 60%  $A_{stim}$ ,  $k_{Exo} = 0$  condition, and output  $\sim 1.7 \text{ W kg}^{-1}$  was observed for the 50% $A_{stim}$ , 30% $k_{SEE}$  (i.e.  $k_{Exo} = 54 \text{ kN m}^{-1}$ ) condition, matching findings for whole ankle  $\bar{P}_{mech}^+$  in a single limb from previous human studies [21] (figure 7(A)). These conditions are highlighted on most contour plots by a white star (figures 3(A), (C) and 6(A)–(C)), and compared directly in figure 7. Similarities between experimental and modeled conditions include little to no change in  $P_{mech}^+$  for the CE, large reductions in  $\bar{P}_{mech}^+$  for both the SEE and whole MTU, with a considerably greater fraction of MTU  $\bar{P}_{mech}^+$  coming from the CE (figure 7(A)), and a reduction in  $\bar{P}_{met}$  (figure 6(A)) when springy assistance was provided. There were also strong qualitative similarities in the time-course of MTU/MTU + Exo force production and MTU/CE excursion dynamics during ground contact (figures 7(B), (C)). The major difference between modeled/experimental data had to do with rate of force onset/offset (figure 7(B)) and CE excursion (figure 7(C)) in late/early stance.



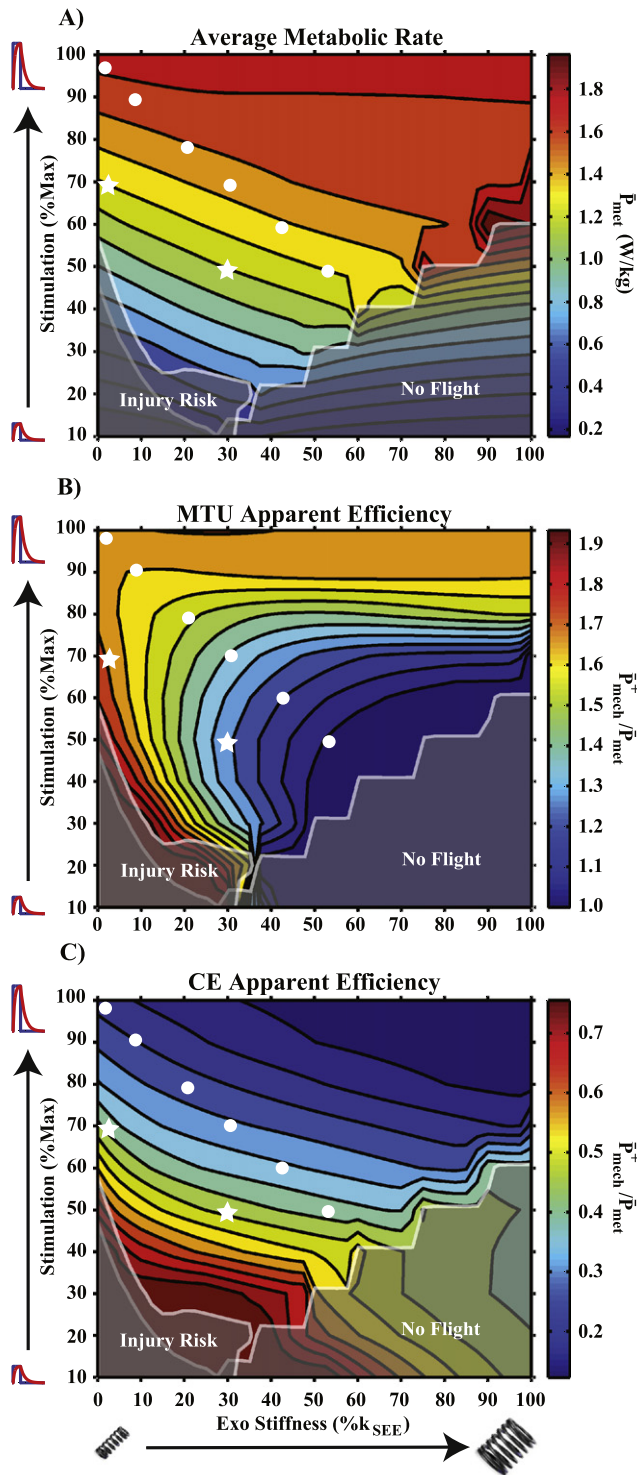


**Figure 6** (A) Average metabolic rate for the modeled CE. Stimulation amplitude was the primary factor governing metabolic cost, as indicated by horizontal contours. (B) Contour plot of MTU apparent efficiency. Note that any application of exoskeleton assistance resulted in reduced apparent efficiency except for stimulation amplitudes  $\geq 90\%$ . (C) Contour plot of CE apparent efficiency (passive + active). In general, decreased stimulation amplitude increased CE apparent efficiency, and adding exoskeleton stiffness decreased CE apparent efficiency.

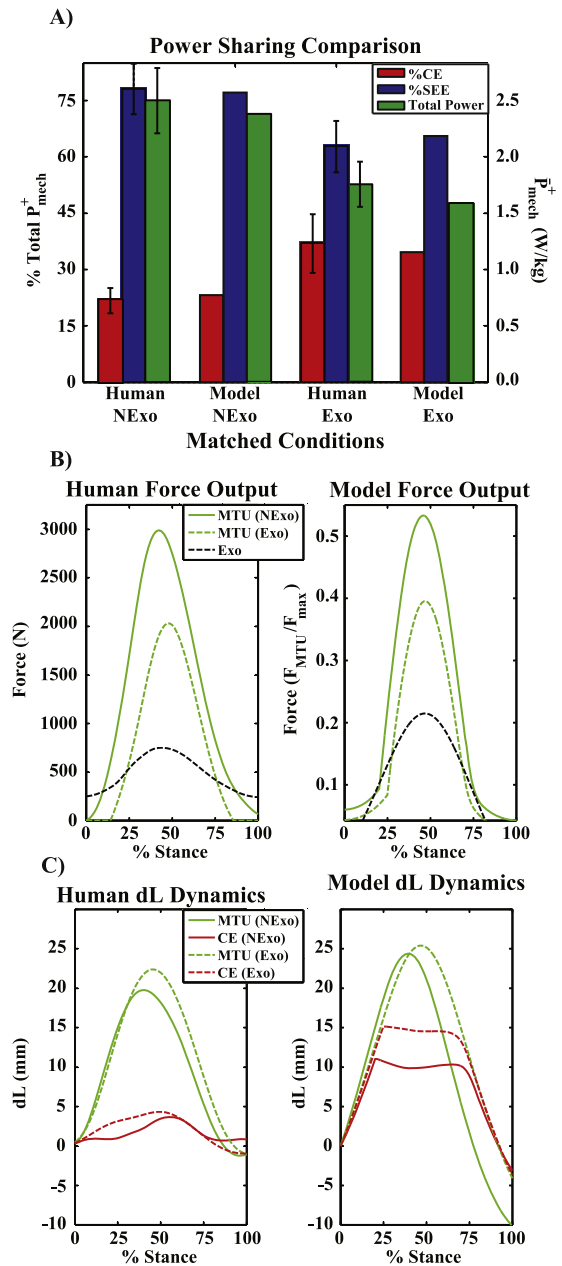


**Figure 7** (A) Comparison of Exoskeleton (Exo) and No Exoskeleton (NExo) conditions from [22] with appropriately matched model conditions (stars in figures 3(A), (C) and 6(A)–(C)). The left axis indicates percent contribution from CE/SEE to total MTU  $\bar{P}_{mech}^+$ . The right axis is total ankle joint/MTU  $\bar{P}_{mech}^+$  for experimental and model studies respectively. Note that an error bar indicating  $\pm 1$  SEM is on all experimental data, and that matched model data fell easily within this range of values. (B) Human (left) and model (right) force versus % stance for matched (star) conditions. Note comparable timescourse of force production for NExo and Exo conditions, as well as reduced peak MTU force when exoskeleton assistance was applied. (C) MTU and CE excursion during stance for experimental (left) and matched model (right) Exo and NExo conditions. Note that both show increased MTU and CE excursion for the Exo condition due to increased CE excursion in early stance, as well as a shift in the timing of peak MTU length relative to stance time.

## Discussion

The intention of this study was to use a simple neuro-mechanical model to understand the impact of springy exoskeleton assistance at the ankle joint. Model predictions agreed well with observation from experimental studies, and provided ample insight into muscle-level mechanisms of neuromechanical and energetic adaptation during spring-assisted hopping [21, 22, 25–27]. Based on model results, we were able to provide general insight into factors influencing system performance, as well as limitations on the benefits a passive device can ultimately provide.

### MTU+ Exo mechanics

Based on observations from previous experimental studies we hypothesized that by increasing exoskeleton stiffness and reducing stimulation amplitude, our model system (MTU + Exo) would be able to maintain a constant  $\bar{P}_{\text{mech}}^+$  output and ‘stiffness’ from an unassisted condition [21, 25–27]. Model findings agreed with this hypothesis, and it was possible to start at any stimulation level  $\geq 60\%$  without exoskeleton assistance, and maintain  $\bar{P}_{\text{mech}}^+$  production by decreasing  $A_{\text{stim}}$  and increasing  $k_{\text{Exo}}$  (figure 3(A)). By following any one of these contours, it was observed that there were nearly identical force–displacement (e.g. ‘stiffness’) dynamics during stance as demonstrated by MTU+Exo workloops from selected points in figure 3(A) (figure 3(B)).

### MTU and SEE mechanics

Our second hypothesis was that, by following a contour of constant MTU+Exo  $\bar{P}_{\text{mech}}^+$ , there should be reduced MTU forces at  $t_{\text{peak}}$  as well as a decrease in SEE and MTU contribution to MTU+Exo  $\bar{P}_{\text{mech}}^+$  [21, 22, 25–27]. By examining figure 4, it can be seen that this is indeed the case. As  $k_{\text{Exo}}$  was increased and  $A_{\text{stim}}$  decreased, contributions to peak MTU+Exo force from MTU were reduced, while those from Exo increased (figure 4(A)). A similar trend emerges for power sharing, where reductions in MTU/SEE  $\bar{P}_{\text{mech}}^+$  were offset by increased output from the Exo (figure 4(B)). Given that the ankle plantar flexor muscle groups depend primarily on inertial dynamics and elastic energy cycling as a means for joint level  $\bar{P}_{\text{mech}}^+$  generation [16, 22, 23], it follows that reduced loading results in reduced  $\bar{P}_{\text{mech}}^+$  production in the SEE and MTU as a whole.

### Muscle mechanics

Our third hypothesis predicted that, in spite of reduced biological loading, average positive power in the CE would remain constant. The predicted mechanism by which this would occur was increased excursions in conjunction with reduced CE forces, which would result in nearly constant CE average positive power production [22]. By examining figure 4(B), it can be seen that, as  $A_{\text{stim}}$  was decreased and  $k_{\text{Exo}}$  increased, CE  $\bar{P}_{\text{mech}}^+$  remained nearly constant, and even increased slightly for  $k_{\text{Exo}} > \sim 20\%k_{\text{SEE}}$  ( $\sim 36 \text{ kN m}^{-1}$ ) conditions (figures 3(C) and 4(B)). Our model also predicted that

this occurred in conjunction with reduced biological loading (figure 4(A)) as well as increased CE excursion (figures 3(D) and 5(A)) and average operating velocity (figure 5(B)) in full agreement with hypothesis (3). Increased excursions also occurred in conjunction with greater values of  $\epsilon_{\text{peak}}$ , many of which were  $> 0$  (i.e.  $l_{\text{CE}} > l_0$ ) (figures 2(A) and 5(A)), resulting in passive CE force generation (figure 4(A)). This coupling of force generation to CE length also played a role in keeping CE  $\bar{P}_{\text{mech}}^+$  at near constant levels (figure 4(B)).

### Energetics of assisted hopping

For our fourth and final hypothesis, we predicted that by following a contour of constant MTU+Exo  $\bar{P}_{\text{mech}}^+$  it would be possible to reduce  $\bar{P}_{\text{met}}$  from the unassisted condition [21, 26]. Following the contour of white dots from figure 3(A), increasing  $k_{\text{Exo}}$  required a reduction in  $A_{\text{stim}}$ , which was the primary determinant of  $\bar{P}_{\text{met}}$  for our modeled data (figure 6(A)). This was in spite of greater average operating velocities (figure 5(B)), and no reduction in  $\bar{P}_{\text{mech}}^+$  output from the CE (figures 3(B) and 4(B)).

Contours of constant MTU+Exo  $\bar{P}_{\text{mech}}^+$  in figure 3(A) all ran into the same problem as  $k_{\text{Exo}}$  increased and  $A_{\text{stim}}$  decreased: there came a point where the system was no longer capable of hopping. In these conditions, the mechanical response of biological and exoskeleton model components to cyclic stimulation was such that they counteracted each other, resulting in force and power production dynamics that did not facilitate a flight phase (figure 2(B)). In order to achieve hopping behavior at higher values of  $k_{\text{Exo}}$  it became necessary to raise  $A_{\text{stim}}$ , and ultimately increase  $\bar{P}_{\text{met}}$  (figures 3(A) and 6(A)). This outcome was in line with observations from Grabowski *et al* (2009), which demonstrated that a more compliant exoskeleton achieved greater reductions in  $\bar{P}_{\text{met}}$  than a stiffer one [26]. Unfortunately, Grabowski *et al* did not record EMG as part of their study, so there is no way of knowing whether or not reduced metabolic benefit in stiffer exoskeletons was accompanied by increased muscle activation as predicted here [26].

Even though there were significant reductions in metabolic rate when  $A_{\text{stim}}$  was reduced in conjunction with increasing  $k_{\text{Exo}}$ , it did not make the biological system as a whole more efficient. In fact, it had the exact opposite effect (figure 6(B)). By applying mechanical assistance and reducing the force burden on the MTU, the ability for an SEE to effectively cycle energy was reduced considerably (figure 4). The ultimate result was a large decrease in MTU apparent efficiency (figure 6(B)) despite concomitant reductions in metabolic rate (figure 6(A)).

This system level trend did not hold at the muscle level, and CE  $\bar{P}_{\text{mech}}^+$  output remained constant as  $\bar{P}_{\text{met}}$  declined with increasing  $k_{\text{Exo}}$  (figure 4(A)). This resulted in muscle  $e_{\text{app}}$  rising from  $\sim 25\%$  in the unassisted condition to  $\sim 40\%$  at the highest level of assistance for the data point in figure 3(A) ( $50\%A_{\text{stim}}$ ,  $k_{\text{Exo}} = 90 \text{ kN m}^{-1}$ ) (figure 6(C)). This increased CE apparent efficiency, however, came with greater  $\epsilon_{\text{peak}}$  values/risk of injury (figure 2(A)) and increased energy cycling in passive CE elements (figure 4(B)).

### Comparison of modeled and experimental data

Despite the simplicity of the model implemented here, it could be compared rather nicely to human joint level data observed in Farris *et al* [21, 22]. By constraining our  $k_{\text{Exo}}$  values based on those used in experimental studies, and sweeping our  $A_{\text{stim}}$  for values of MTU  $\bar{P}_{\text{mech}}^+$  observed experimentally, we identified a point of best fit for the Exo with no spring ( $A_{\text{stim}} = 70\%$  of max,  $k_{\text{Exo}} = 0\%k_{\text{SEE}}$ ) and Exo with spring ( $A_{\text{stim}} = 50\%$  of max,  $k_{\text{Exo}} = 30\%k_{\text{SEE}}$ ) conditions from [21, 22] for hopping at 2.5 Hz (figure 7(A), stars in figures 3(A),(C) and 6). These points maintained constant MTU + Exo  $\bar{P}_{\text{mech}}^+$  (figure 3(A)), reduced  $A_{\text{stim}}$  and  $\bar{P}_{\text{met}}$  requirements from unassisted (figure 6(A)), and traded reduced CE force (figure 7(B)) for increased excursion (figure 7(C)) to keep  $\bar{P}_{\text{mech}}^+$  constant (figure 3(C)). Direct comparisons of muscle/tendon mechanics was difficult, since experimental data were *only* for the soleus MTU, and our model has all three plantarflexors lumped into a single monoarticular MTU. We did, however, directly compare % of total  $\bar{P}_{\text{mech}}^+$  from CE/SEE in both studies, and found a quantitative match easily within  $\pm 1$  Standard Error of the Mean (SEM) of experimental data (figure 7(A)).

There were, however, some shortcomings of model findings as well. Most notably, our model predicted significant passive CE stretch in early stance (figure 7(C)). This was not observed in human studies, where the ability to actively modulate MTU position with antagonist muscles (i.e. tibialis anterior) and knee flexion likely work together to limit CE lengthening in early stance (figure 7(C)). Secondly, while qualitative trends in metabolic demand agreed (i.e.  $\bar{P}_{\text{met}}$  reduced with Exo, figure 6(A)), the model underestimated values of reductions in whole body metabolic cost attributed to reduced plantar-flexor loads from [22]. Again, this was likely attributable to model simplifications, which do not allow for bi-articular plantar flexors (i.e. medial and lateral gastrocnemii) that contribute to knee joint mechanical demands in humans [21].

### Conclusions and the case for optimal exoskeleton stiffness for bouncing gait

With all of these model predictions and simplifications in mind, the question now becomes one of optimization. How can metabolic benefits, MTU and CE efficiency, and risk of injury all be balanced to best assist a compliant MTU? Was there a point or region in parameter space where detrimental and beneficial aspects can be balanced to achieve an idealized outcome? We are confident that humans would follow a path through our parameter space that kept Exo + MTU stiffness and average positive power nearly constant [27] (figures 3(A)–(B) and 4(A)), maintained near constant CE positive power [22] (figures 3(C)–(D) and 4(A)), reduces muscle activation [21, 22, 25], and allowed for reduced metabolic energy consumption [21, 22, 26] (figure 6(A)). A significant region of parameter space remained accessible even with these restrictive criteria in place, and all of these regions terminated at a point where flight was no longer

achieved or injury risk was too great beyond some terminal increase in  $k_{\text{Exo}}$ /reduction in  $A_{\text{stim}}$  (figure 3(A)). In every case, the only way to sustain hopping beyond this point was to increase  $A_{\text{stim}}$  in conjunction with increasing  $k_{\text{Exo}}$ , ultimately resulting in increased metabolic cost (figure 6(A)) and average positive power from the MTU + Exo system (i.e. enhanced performance) (figure 3(A)). This, again, agrees with observed trends in human data [26], and leads us to the conclusion that springy assistance will be optimized for metabolic benefit when muscle activation is minimized and MTU + Exo power/stiffness remains consistent with the baseline/unassisted condition.

This model also made a second interesting prediction: by increasing assistance beyond the point of optimal metabolic benefit, it was possible to obtain better mechanical performance (i.e. hop height, Exo + MTU positive power) than the biological system alone (figures 2(B) and 3(A)). These regions of enhanced performance were also coincident with reduced CE positive power (figure 3(C)) and injury risk (figure 2(A)), as well as an increased metabolic cost relative to conditions where expenditure is minimized (figure 6(A)). This agrees with observations from Grabowski *et al*, where increased performance/hop height was also accompanied by greater variability in touchdown position, indicating that greater performance may come at the cost of reduced stability [26]. In conclusion, our model does predict that metabolic and mechanical performance benefits can be achieved simultaneously, but that neither is likely to be optimal while the other persists in a compliant MTU.

### Future directions

By examining the interplay of reflex feedback, feed-forward control, and a wearable device, we hope to better understand how design of assistive devices may be optimized to achieve a desired outcome, be it reduced metabolic cost or enhanced performance. Towards this end, future modeling work will integrate simulated spinal cord reflex pathways in conjunction with feed-forward control to further explore the possibilities and limitations of spring-based assistive exoskeletons. Given the possible variation in muscle fascicle length, velocity and force production dynamics observed in this study, it seems likely that feedback through spindle and/or golgi tendon organs could play a role in shaping adaption to steady state dynamics in the context of external assistance. Finally, future experimental work will include studies of human hopping for a range of exoskeleton stiffness' with instrumentation similar to Farris *et al* [21, 22] to better understand neural and metabolic adaptation to springy exoskeletons, and either verify or refute predictions made here regarding tradeoffs between reductions in metabolic cost and enhanced mechanical performance.

### Acknowledgments

This study was in part funded by US Israel Binational Science Foundation Start Up Grant 2011152 awarded to G S Sawicki.

## References

- [1] Ferris D P 2009 The exoskeletons are here *J. Neuroeng. Rehabil.* **6** 17
- [2] Kawamoto H, Suwoong L, Kanbe S and Sankai Y 2003 *Power Assist Method for HAL-3 using EMG-based Feedback Controller* **1642** pp 1648–53
- [3] Zoss A B, Kazerooni H and Chu A 2006 Biomechanical design of the Berkeley lower extremity exoskeleton (BLEEX) *IEEE/ASME Trans. Mechatronics* **11** 128–38
- [4] Ferris D P and Lewis C L 2009 Robotic lower limb exoskeletons using proportional myoelectric control *Conf. Proc. IEEE Eng. Med. Biol. Soc. (2009)* pp 2119–24
- [5] Mooney L M, Rouse E J and Herr H M 2014 Autonomous exoskeleton reduces metabolic cost of human walking during load carriage *J. Neuroeng. Rehabil.* **11** 80
- [6] Hocoma ([www.hocoma.com/en/products/lokomat/](http://www.hocoma.com/en/products/lokomat/))
- [7] Malcolm P, Derave W, Galle S and De Clercq D 2013 A simple exoskeleton that assists plantarflexion can reduce the metabolic cost of human walking *PLoS One* **8** e56137
- [8] Wehner M *et al* 2013 *A Lightweight Soft Exosuit for Gait Assistance (Karlsruhe, Germany, May 6–10 2013)* pp 3362–9
- [9] Wiggin M B, Sawicki G S and Collins S H 2011 *An Exoskeleton Using Controlled Energy Storage and Release to Aid Ankle Propulsion* pp 1–5
- [10] Hasegawa Y and Ogura K 2013 First report on passive exoskeleton for easy running: PEXER IV 1–6
- [11] Elliot G, Sawicki G S, Marecki A and Herr H 2013 The biomechanics and energetics of human running using an elastic knee exoskeleton (24–26 June 2013) pp 1–6
- [12] Geyer H, Seyfarth A and Blickhan R 2006 Compliant leg behaviour explains basic dynamics of walking and running *Proc. Biol. Sci.* **273** 2861–7
- [13] Holt K G, Hamill J and Andres R O 1990 The force-driven harmonic-oscillator as a model for human locomotion *Hum. Mov. Sci.* **9** 55–68
- [14] Blickhan R 1989 The spring-mass model for running and hopping *J. Biomech.* **22** 1217–27
- [15] Srinivasan M 2011 Fifteen observations on the structure of energy-minimizing gaits in many simple biped models *J. R. Soc. Interface.* **8** 74–98
- [16] Farris D J and Sawicki G S 2012 Human medial gastrocnemius force–velocity behavior shifts with locomotion speed and gait *Proc. Natl. Acad. Sci. USA* **109** 977–82
- [17] Lichtwark G A, Bougoulias K and Wilson A M 2007 Muscle fascicle and series elastic element length changes along the length of the human gastrocnemius during walking and running *J. Biomech.* **40** 157–64
- [18] Lichtwark G A and Wilson A M 2008 Optimal muscle fascicle length and tendon stiffness for maximising gastrocnemius efficiency during human walking and running *J. Theor. Biol.* **252** 662–73
- [19] Lichtwark G A and Wilson A M 2007 Is Achilles tendon compliance optimised for maximum muscle efficiency during locomotion? *J. Biomech.* **40** 1768–75
- [20] Fukunaga T *et al* 2001 *In vivo* behaviour of human muscle tendon during walking *Proc. Biol. Sci.* **268** 229–33
- [21] Farris D J and Sawicki G S 2012 Linking the mechanics and energetics of hopping with elastic ankle exoskeletons *J. Appl. Physiol.* **113** 1862–72
- [22] Farris D J, Robertson B D and Sawicki G S 2013 Elastic ankle exoskeletons reduce soleus muscle force but not work in human hopping *J. Appl. Phys.* **115** 579–85
- [23] Takeshita D *et al* 2006 Resonance in the human medial gastrocnemius muscle during cyclic ankle bending exercise *J. Appl. Physiol.* **101** 111–8
- [24] Dean J C and Kuo A D 2011 Energetic costs of producing muscle work and force in a cyclical human bouncing task *J. Appl. Physiol.* **110** 873–80
- [25] Ferris D P, Bohra Z A, Lukos J and Kinnaird C R 2006 Neuromechanical adaptation to hopping with an elastic ankle-foot orthosis *J. Appl. Physiol.* **100** 163–70
- [26] Grabowski A M and Herr H M 2009 Leg exoskeleton reduces the metabolic cost of human hopping *J. Appl. Physiol.* **107** 670–8
- [27] Chang Y H, Roiz R A and Auyang A G 2008 Intralimb compensation strategy depends on the nature of joint perturbation in human hopping *J. Biomech.* **41** 1832–9
- [28] Hof A L, Van Zandwijk J P and Bobbert M F 2002 Mechanics of human triceps surae muscle in walking, running and jumping *Acta Physiol. Scand.* **174** 17–30
- [29] Alexander R M 2002 Tendon elasticity and muscle function *Comp. Biochem. Physiol. A* **133** 1001–11
- [30] Farley C T and Morgenroth D C 1999 Leg stiffness primarily depends on ankle stiffness during human hopping. *J. Biomech.* **32** 267–73
- [31] Zajac F E 1989 Muscle and tendon: properties, models, scaling, and application to biomechanics and motor control *Crit. Rev. Biomed. Eng.* **17** 359–411
- [32] Rubenson J, Pires N J, Loi H O, Pinniger G J and Shannon D G 2012 On the ascent: the soleus operating length is conserved to the ascending limb of the force–length curve across gait mechanics in humans *J. Exp. Biol.*
- [33] Haeufle D F, Grimmer S and Seyfarth A 2010 The role of intrinsic muscle properties for stable hopping—stability is achieved by the force–velocity relation *Bioinspir. Biomim.* **5** 16004
- [34] Robertson B D and Sawicki G S 2014 Exploiting elasticity: modeling the influence of neural control on mechanics and energetics of ankle muscle–tendons during human hopping *J. Theor. Biol.* **353C** 121–32
- [35] Carrier Dr H N C and Earls K D 1994 Variable gearing during locomotion in the human musculoskeletal system *Science* **265** 651–3
- [36] Biewener A A, Farley C T, Roberts T J and Temaner M 2004 Muscle mechanical advantage of human walking and running: implications for energy cost *J. Appl. Physiol.* **97** 2266–74
- [37] Winters J M and Stark L 1988 Estimated mechanical properties of synergistic muscles involved in movements of a variety of human joints *J. Biomech.* **21** 1027–41
- [38] Raasch C C, Zajac F E, Ma B and Levine W S 1997 Muscle coordination of maximum-speed pedaling *J. Biomech.* **30** 595–602
- [39] Fukunaga T *et al* 1992 Physiological cross-sectional area of human leg muscles based on magnetic resonance imaging *J. Orthop. Res.* **10** 928–34
- [40] Lieber R L and Friden J 1999 Mechanisms of muscle injury after eccentric contraction *J. Sci. Med. Sport* **2** 253–65
- [41] Lieber R L and Friden J 1993 Muscle damage is not a function of muscle force but active muscle strain *J. Appl. Physiol.* **74** 520–6
- [42] Morgan D L and Allen D G 1999 Early events in stretch-induced muscle damage *J. Appl. Physiol.* **87** 2007–15
- [43] Alexander R M 1997 Optimum muscle design for oscillatory movements *J. Theor. Biol.* **184** 253–9
- [44] Ma S P and Zahalak G I 1991 A distribution-moment model of energetics in skeletal muscle *J. Biomech.* **24** 21–35
- [45] Krishnaswamy P, Brown E N and Herr H M 2011 Human leg model predicts ankle muscle–tendon morphology, state, roles and energetics in walking *PLoS Comput. Biol.* **7** e1001107